RESEARCH ARTICLE SUMMARY

CHEMISTRY AUTOMATION

Autonomous, multiproperty-driven molecular discovery: From predictions to measurements and back

Brent A. Koscher†, Richard B. Canty†, Matthew A. McDonald†, Kevin P. Greenman, Charles J. McGill, Camille L. Bilodeau, Wengong Jin, Haoyang Wu, Florence H. Vermeire, Brooke Jin, Travis Hart, Timothy Kulesza, Shih-Cheng Li, Tommi S. Jaakkola, Regina Barzilay, Rafael Gómez-Bombarelli, William H. Green, Klavs F. Jensen*

INTRODUCTION: The discovery of small molecules with desired functional properties is critical to advances in health, energy, and sustainability. The process is conducted through often slow, laborious, iterative design-make-test-analyze (DMTA) cycles. Emerging machine learning (ML) tools can generate new candidate molecules, predict their properties, and propose reaction pathways with computer-aided synthesis planning (CASP). Progress in chemical automation can enable chemical synthesis and characterization with minimal human intervention after a manual setup. For example, automated feedback-guided chemistry platforms have demonstrated chemical optimization within narrow, well-defined classes of reactions.

RATIONALE: Integrating ML generative algorithms, ML property prediction, CASP, robotics, and automated chemical synthesis, purification, and characterization into a DMTA workflow can lead to the development of autonomous chemical discovery platforms able to operate across varied chemical spaces without manual reconfiguration. An ideal property-focused discovery platform would propose and synthesize molecules to enrich ML generative and property models and ultimately discover top-performing molecules. In reality, it is necessary to exclude reactions that the available automation hardware cannot safely execute.

RESULTS: Toward autonomous discovery, we demonstrate an integrated DMTA cycle that iteratively proposes, realizes, and characterizes molecules to explore chemical spaces guided only by prediction tools. Four molecular scaffolds with potential applications as organic dyes serve as exploration case studies, whereas a fifth scaffold demonstrates the platform-exploiting refined ML models to optimize dye properties. Dye-like molecules constitute a compelling test case as fundamental properties are readily measurable and their realiza… involves multistep synthesis by a wide varie… chemical transformations. The platform automatically characterized three target properties—absorption maximum (λ_{max}), octanol-water partition coefficient ($\log K_{ow}$), and photooxidative stability ($\log k_{deg}$)—and used them to refine model predictions and inform future experiment selection.

A graph-completion generative model designs candidate molecules, which are evaluated with an ML model for each of the three properties. A CASP tool proposes multistep synthetic recipes, which are executed by an automated liquid handler, batch reactors, high-performance liquid chromatography (HPLC), and robotic arms. A plate reader measures absorption spectra, calibrated HPLC retention times provide water-octanol partition coefficients, and a simulated solar light source combined with the plate reader quantifies photooxidative degradation. The measured molecular properties are automatically fed back to retrain the property prediction models, completing one step of the automated DMTA cycle. Initially, the platform is highly uncertain about each scaffold (i.e., the ML prediction models have significant model errors), so it chooses to realize the simplest derivatives to anchor property predictions. Subsequent iterations favor more synthetically complex derivatives to fill gaps in the learned chemical space. Three iterations were sufficient for the ML model deviations to approach experimental uncertainty and enable exploitation. Human involvement was limited to setting and adjusting objectives, providing requested materials, and occasionally fixing unrecoverable errors such as clogging of the HPLC unit.

CONCLUSION: We have demonstrated a DMTA cycle that explores chemical space and exploits known chemical structures without manual experimentation. The platform proposed, synthesized, and characterized 303 unreported dye-like molecules spread across four exploration scaffolds and one exploitation scaffold. The integrated platform can explore unknown structure-property spaces by searching for structures with desired properties (hits) and can exploit characterized structure-property spaces by optimizing structures of promising candidates (leads). Further development of closed-loop integrated platforms promises to accelerate molecular discovery. ■

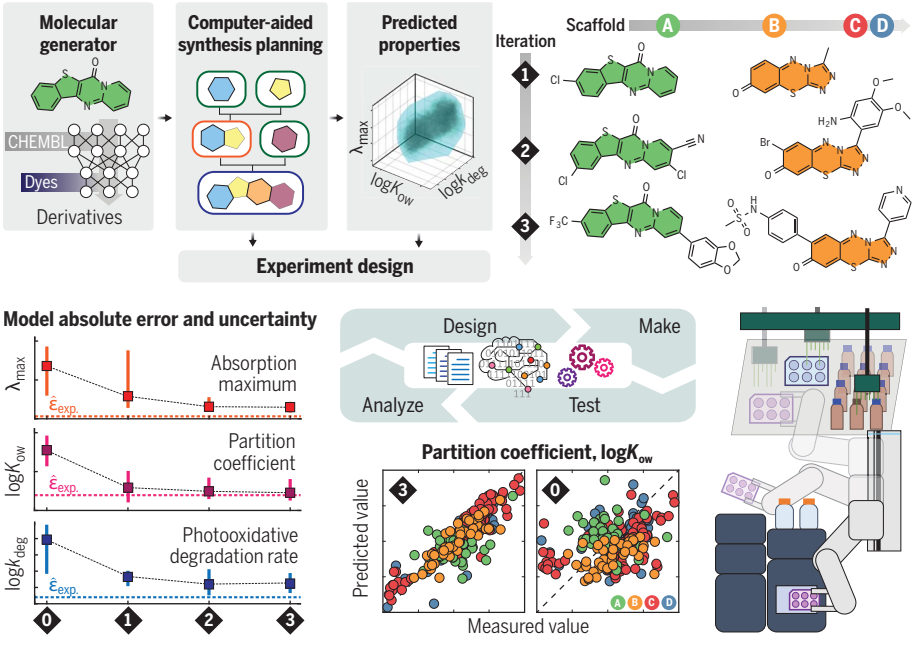

Autonomous molecular discovery. A suite of machine learning tools iteratively plans experiments to learn about a structure-property space defined by molecular dye scaffolds. $\hat{\varepsilon}_{exp.}$, mean experimental error.

The list of author affiliations is available in the full article online.
*Corresponding author. Email: kfjensen@mit.edu
†These authors contributed equally to this work.
Cite this article as B. Koscher *et al.*, *Science* **382**, eadi1407 (2023). DOI: 10.1126/science.adi1407

RESEARCH ARTICLE

CHEMISTRY AUTOMATION

Autonomous, multiproperty-driven molecular discovery: From predictions to measurements and back

Brent A. Koscher[1]†, Richard B. Canty[1]†, Matthew A. McDonald[1]†, Kevin P. Greenman[1], Charles J. McGill[1], Camille L. Bilodeau[1], Wengong Jin[2], Haoyang Wu[1], Florence H. Vermeire[1], Brooke Jin[1], Travis Hart[1], Timothy Kulesza[1], Shih-Cheng Li[1], Tommi S. Jaakkola[3], Regina Barzilay[3], Rafael Gómez-Bombarelli[4], William H. Green[1], Klavs F. Jensen[1]*

A closed-loop, autonomous molecular discovery platform driven by integrated machine learning tools was developed to accelerate the design of molecules with desired properties. We demonstrated two case studies on dye-like molecules, targeting absorption wavelength, lipophilicity, and photooxidative stability. In the first study, the platform experimentally realized 294 unreported molecules across three automatic iterations of molecular design-make-test-analyze cycles while exploring the structure-function space of four rarely reported scaffolds. In each iteration, the property prediction models that guided exploration learned the structure-property space of diverse scaffold derivatives, which were realized with multistep syntheses and a variety of reactions. The second study exploited property models trained on the explored chemical space and previously reported molecules to discover nine top-performing molecules within a lightly explored structure-property space.

The efficient prediction, realization, and validation of small molecules, polymers, and materials with desirable functional properties is needed to accelerate advances in medicine (*1*, *2*), materials (*3*–*5*), and sustainability (*6*, *7*). This work focuses on organic small molecules that must manifest multiple distinct properties simultaneously, constraining molecular design and increasing structural complexity. Emerging predictive tools can quickly generate new candidate molecules (*8*–*13*), predict the performance of candidates (*11*, *14*–*16*), and propose practical reaction pathways (*17*–*21*); meanwhile, chemical automation can now dependably conduct experiments with minimal human intervention after an initial setup phase. Integrating generative algorithms, computer-aided synthesis planning (CASP), iteratively updated large datasets, and automated chemical synthesis, purification, and characterization for each step of the design-make-test-analyze (DMTA) cycle all into a single workflow could improve experiment efficiency and ultimately enable autonomous chemical discovery. Automated feedback-guided chemistry platforms have demonstrated molecular chemical discovery and optimization within narrow classes of reactions, performing iterative cross-coupling reactions (*8*, *22*), rediscovering reactivity (*23*), optimizing single reactions (*24*–*26*), and driving enzyme-assisted carbohydrate synthesis (*27*). Although these demonstrations highlight the potential of integrating predictive tools and chemical automation, their specialized implementations restrict the types of chemistry executed, the types of structures that can be realized, and notably, the chemical spaces that can be explored by these platforms.

Currently, there is a gap between the general nature of chemical prediction tools, retrosynthesis planning and property prediction, and the specialized nature of existing chemical automation platforms for the synthesis of small molecules. Closing this gap can lead to the development of autonomous chemical discovery platforms that can pivot between different discovery spaces without the need for manual reconfiguration. In the idealized case, a molecular property–focused discovery platform would propose and evaluate synthesizable molecules by using all known reactions to avoid constraints beyond those imposed by multiproperty spaces. This work narrows the gap by demonstrating an integrated platform to iteratively propose, realize, and validate molecules to explore chemical spaces guided only by prediction tools. In practice, a minimal set of reactions that cannot be safely executed by the selected automation hardware and engineering controls must be excluded. The platform integrates general chemical tools to automatically propose diverse molecules, plan synthetic pathways, execute multistep reaction pathways, purify target molecules, and characterize the performance of isolated molecules to learn about unfamiliar chemical spaces (Fig. 1A). By weighing potential challenges with each workflow in the DMTA cycle, the platform holistically evaluates the utility of a datapoint to the models against the experimental complexities required to realize a proposed molecule. Although this is analogous to how a trained chemist might approach chemical discovery, the autonomous platform can perform this evaluation on multiple properties and multiple experimental plans for thousands to millions of molecules simultaneously. As a result of this holistic consideration, the platform chooses unadorned structures to probe unexplored chemical spaces and builds more complex derivatives to optimize the properties of familiar spaces.

To initiate the automated DMTA cycle, candidate structures can be generated by using molecular generation workflows based on genetic algorithms (*8*, *9*), reinforcement learning (*10*–*12*), or conditional generation (*13*, *28*). Plausible pathways to realize candidates can be proposed by using retrosynthetic planning packages, such as ASKCOS (*17*, *18*), Synthia (*19*, *29*), IBM RXN (*20*), and AiZynthFinder (*21*). The properties of candidates can be predicted with quantitative structure-activity relationship models or statistical models such as Chemprop, a message-passing neural network (*16*). Molecules can be realized with advances in chemical automation such as reconfigurable high-throughput platforms (*18*, *24*, *30*) equipped with hardware to access diverse reaction conditions (*31*) and molecular property characterization (*7*, *32*). Such platforms have been used to discover novel chemical transformations (*32*, *33*), optimize reactions (*34*, *35*), and develop functional materials (*7*, *26*, *33*). This work integrates these tools to demonstrate a platform that can autonomously drive molecular discovery.

We demonstrated the platform (Fig. 1B) in two molecular discovery use cases for small molecule organic dyes: (i) exploration of unknown chemical spaces and (ii) exploitation of a known chemical space. The platform executes and automatically adjusts workflows as needed, with human intervention being limited to managerial (error recovery) and custodial (providing consumables) actions, both during and between iterations. A complete discussion on required human action is provided in the supplementary materials (SM8). Platform flexibility is crucial to execute multistep reaction pathways containing the breadth of reaction classes (Fig. 1C) needed to realize candidates covering the desired property space. We validated the platform's capabilities by targeting molecular dyes, a model system with diverse chemistry and complex molecular properties. During two case studies, the platform attempted over 3000 reactions, with more than 1000 yielding the predicted reaction product, completing multistep reaction pathways for 303 unreported molecules (i.e., without CAS

[1]Department of Chemical Engineering, Massachusetts Institute of Technology, Cambridge, MA, USA. [2]Broad Institute of MIT and Harvard, Cambridge, MA, USA. [3]Computer Science and Artificial Intelligence Laboratory, Massachusetts Institute of Technology, Cambridge, MA, USA. [4]Department of Materials Science and Engineering, Massachusetts Institute of Technology, Cambridge, MA, USA.
*Corresponding author. Email: kfjensen@mit.edu
†These authors contributed equally to this work.

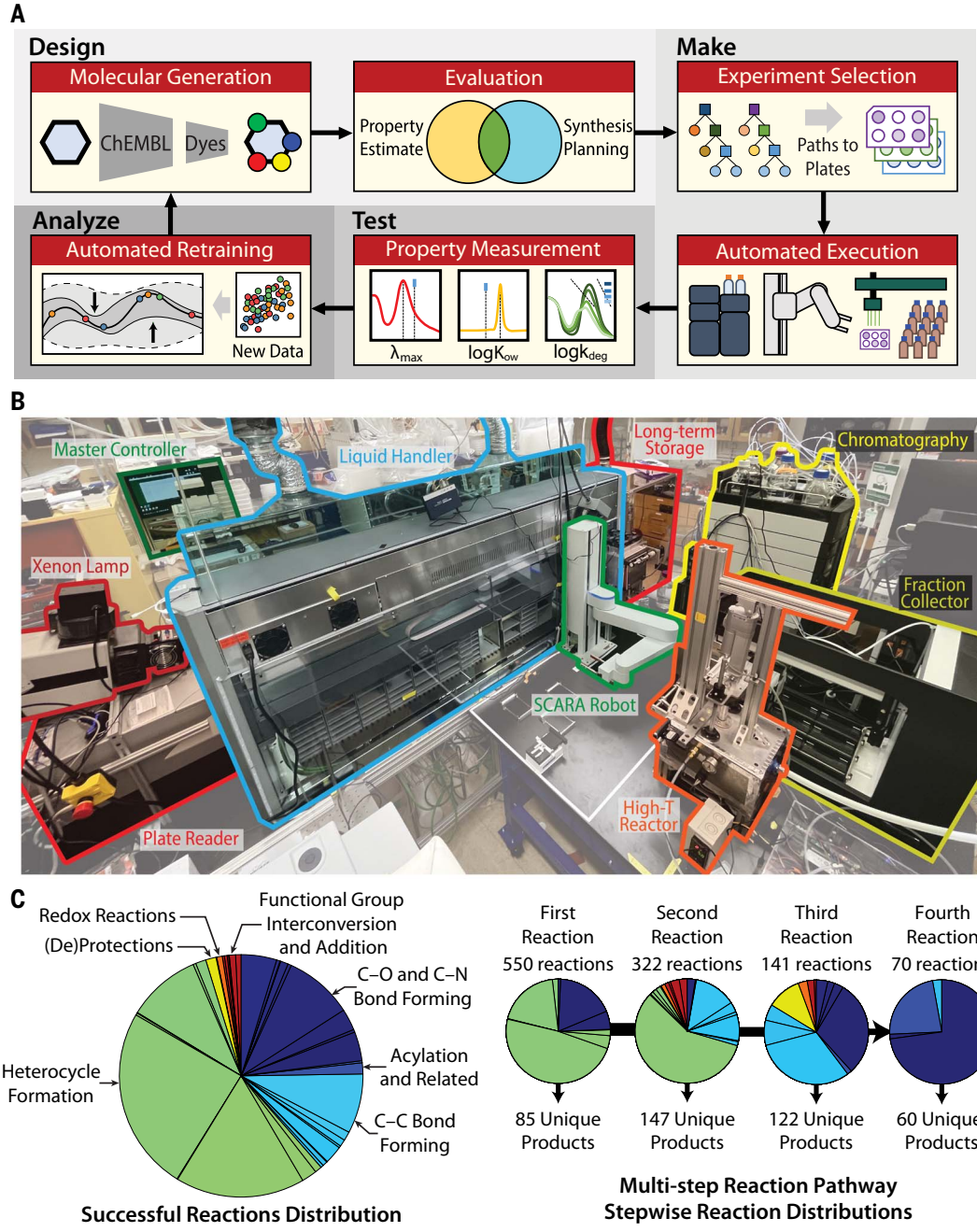

Fig. 1. Overview of the integrated platform and reactions predicted and successfully executed by the platform. (**A**) Illustrations of the key workflow components of the integrated platform and how each component fits into the DMTA cycle in which the properties tested are wavelength of maximum absorption (λ_{max}), octanol-water partition coefficient ($\log K_{ow}$), and rate of photooxidative degradation ($\log k_{deg}$). (**B**) Layout of the physical hardware of the experimental platform. (**C**) Stepwise breakdown of the classes of different reaction classes automatically executed by the platform during the exploration case study. The four smaller pie charts show the change in the reaction class distribution as a function of the reaction step number. Not all executed pathways have the same number of reactions, leading to fewer reactions at later step numbers. A detailed breakdown of the subreaction classes is given in fig. S5.

registry numbers prior to publication). For both case studies, the absorption maximum, partition coefficient, and photooxidative stability were the targeted properties, and the platform automatically measured and recorded each property to refine model predictions and inform future experiment selection.

Front-end predictions

The platform is tasked with either learning the properties of a chemical space of interest or realizing top-performing molecules within a chemical space containing existing examples. Before experiments can be executed, the platform must develop an experimental plan by proposing candidate structures, planning reaction pathways and reaction conditions, predicting candidate properties, and selecting candidates to realize (Fig. 1A, design). These prediction tasks are modular and can be exchanged to accommodate different objectives.

Candidate structures are proposed by using a hierarchical graph-completion model (*34*), which takes a molecule scaffold as input and completes the molecular graph with learned motifs, encoding and decoding full motifs at once rather than atom by atom. The model was first pretrained on ChEMBL (*35*) to learn general organic chemistry rules and then fine-tuned on a curated set of dye molecules (supplementary materials, SM2) to complete input scaffolds with diverse dye-like structural motifs. Graph completion proposes molecules spanning the multiproperty space of dye molecules and tends to generate more realistic and feasible structures compared with other molecular generation approaches (*8*–*13*, *28*). Graph completion also has the benefit of generating diverse derivatives while preserving the input scaffold, enabling exploration within a local chemical structure family. The technique adds common functional groups such as dialkylamino or cyano groups, whereas a graph-to-graph translation model we tested added polyene chains or boron inspired by high-performing cyanine

and BODIPY dyes, respectively, without conserving the central scaffold.

For each of the generated candidate molecules, multiple synthesis pathways are automatically planned and proposed by using ASKCOS (*17*, *18*), which makes template-based retrosynthesis recommendations with reaction templates extracted from large reaction databases. Reaction templates are iteratively applied in a tree search to propose reaction pathways that terminate at available reagents, connecting available starting materials, chemicals, and generated structures. A set of preferred-vendor chemical catalogs—containing SMILES, package sizes, vendor product IDs, and prices—and our in-lab inventory formed the set of reagents available to ASKCOS. Reaction pathways that do not terminate at available reagents within five reaction steps were discarded from consideration (supplementary materials, SM3). The majority of reaction pathways for generated molecules require multiple reactions, often from different reaction classes. By executing multistep reaction pathways, more of the multidimensional property space becomes accessible (Fig. 2A, volume), and moreover, there are more candidate options within the space (Fig. 2A, density). Single-step syntheses cover only 30% of the space accessible with five reaction steps and have 1000-fold fewer candidate options (Fig. 2A). In our property space of interest, molecules requiring more than five reaction steps did not further expand the volume of property space but did increase complexity and resource requirements. As a result, we set a limit of five reaction steps for the case studies presented, but other spaces may require more steps for adequate exploration.

Retrosynthesis planning also serves to determine which generated candidates are considered synthesizable. Depending on the heterocyclic scaffold, 10 to 20% of generated molecules return synthesis pathways terminating at buyable starting materials. Retrosynthesis planning is the most time intensive front-end prediction needed to create an experimental plan. Unrealistic molecules suggested by molecular generation are often filtered with synthesizability proxy metrics (*36*–*39*); however, commonly used metrics did not increase the quality of reaction planning (fig. S2), and therefore, they were not used to prefilter candidate structures during exploration. The continued development of more efficient methods to recommend candidates and pathways simultaneously would increase platform planning throughput (*39*).

Reaction conditions are recommended by ASKCOS by using a neural network model trained on a large set of literature reaction conditions (*40*). The recommendation of reaction conditions can be challenging as necessary reagents, catalysts, cocatalysts, solvents, and reaction temperature must be predicted simultaneously. To assist ASKCOS, we defined a set of rules for the 100 most popular chemical transformation templates (supplementary materials, SM3) against which ASKCOS predictions are checked. These rules identify common problems such as not recommending all required reagents for well-known reactions (e.g., recommendation of phosphorus ligand, base, solvent, and palladium source for cross-coupling reactions) or recommending outdated catalysts when improved catalysts are known. Reaction condition recommendations that did not match the predefined rules were automatically either corrected when a single required chemical was missing or removed from consideration when multiple issues were present. Although defining rules for known reactions can help fix some problematic recommendations, the continued development of reaction condition models is needed to increase the success rate of platform-executed reactions. Pathways containing a reaction without any valid recommended conditions are automatically discarded. The combination of reaction pathways and reaction conditions form experimental plans for each of the generated molecules (Fig. 2B).

For candidates with an experimental plan, their dye-like properties were predicted by using a set of Chemprop (*14*, *15*) property prediction models: wavelength of maximum absorption, partition coefficient, and photooxidative

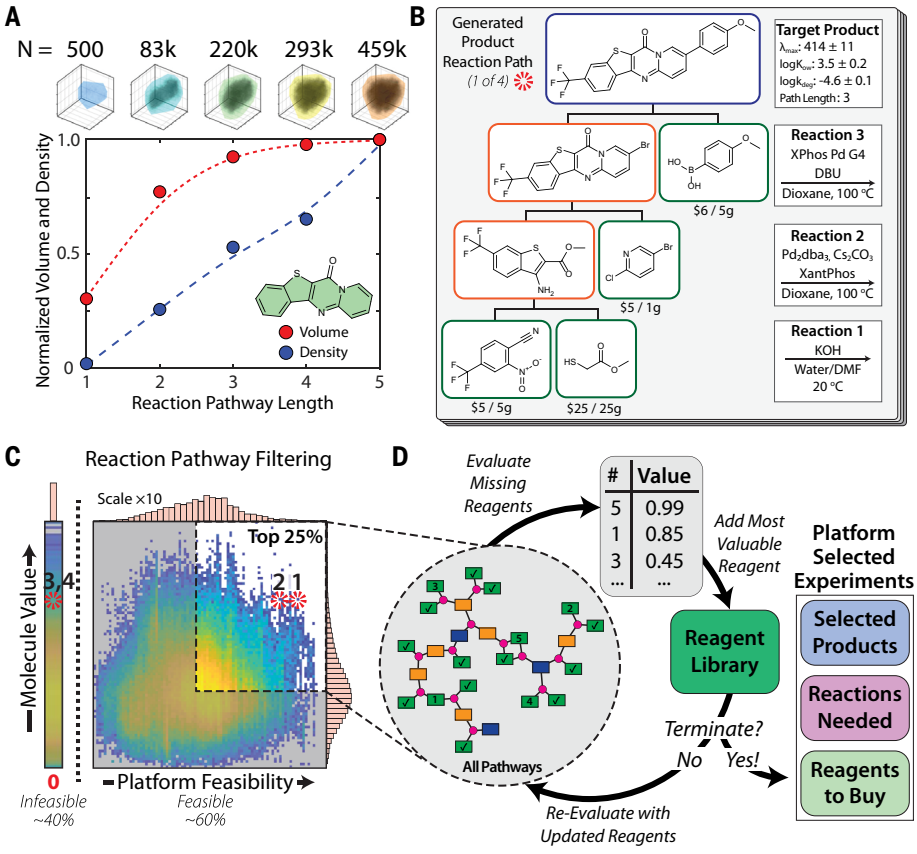

Fig. 2. Product and reaction pathway selection. (**A**) Property space (λ_{max}, logK_{ow}, and logk_{deg}) convex hull volume (red) and density of candidates (blue) for the BTPP scaffold shown in the exploration case study as a function of reaction pathway length. Dashed lines are splines provided as a guide to the eye. The convex hull volume at each pathway length has units of wavelength, logK_{ow}, and logk_{deg} normalized to the volume at a reaction pathway length of 5. The density is the similarly normalized number of candidates per unit of volume. (**B**) Example of an experimental plan to be scored, including the predicted property values (units of nanometers for λ_{max} and units of $\log_{10}(s^{-1})$ for logk_{deg}) and reaction pathways, and the top-ranked reaction context. The target candidate molecule had four experimental plans for consideration [red stars in (C)]. (**C**) Evaluation of experimental plan scores considering the platform feasibility of the proposed reaction pathway and candidate molecule value. The space is separated by infeasible (left) and feasible (right) candidate pathways. Candidates were deemed infeasible if they required platform-inaccessible reaction conditions or reagents. The color scale represents the density of candidates, increasing from low (blue) to high (yellow). (**D**) Decision cycle for additional reagents to buy by evaluating the products and reaction pathways they enable. Upon terminating, the platform has selected products to make, reactions to execute, and reagents to purchase. Reaction pathways connect buyable reactants (green) to intermediate products (orange) and target final products (blue).

degradation rate. Chemprop is lightweight and fast, so an ensemble of models can be automatically retrained from the whole dataset with each batch of experimental data (supplementary materials, SM4) (*14*–*16*, *41*). The ensemble variance is used as a proxy for model uncertainty to further inform molecule selection. Each of the models was initially trained on datasets of different sizes: 26,400 experimental absorption maxima from a compiled literature dataset (*42*), 23,500 experimental partition coefficient values also from a compiled literature dataset (*43*), and 85 experimental photooxidative degradation rates measured in house for a set of common molecular dyes (supplementary materials, SM11). Because of the small size of the third dataset, we used a random forest model implemented through Chemprop to predict photooxidative degradation rates (supplementary materials, SM4). On every iteration of the DMTA cycle, ensembles of models were trained with experimental data measured on realized molecules and the initial datasets. Subsequent rounds of property predictions were automatically made with the most recent property model version, and the predicted properties and uncertainties were used in conjunction with experimental plans to select the next iteration of candidates for experimental realization.

Selecting candidate molecules is challenging, as it involves a tradeoff between optimizing multiple properties and executing a successful synthesis. Additionally, both syntheses and properties are predictions from statistical models with varying uncertainty, which further complicates selection. For an input scaffold, there can be thousands of candidates, each with up to 10 pathways, and thousands of reagents to consider across all pathways. Reactions that require inaccessible conditions, require reagents without vendor information, or involve blacklisted reagents are automatically identified and removed from consideration. Two general categories of infeasible reactions are those requiring inaccessible reagents (no platform-known source or prohibitively expensive) and those involving platform-incompatible reaction conditions (reaction temperatures outside the range of 5° to 200°C or the use of reagents that cannot be safely handled by platform). Incompatible reagents include reactive gases (e.g., hydrogen and carbon monoxide), solid reagents that do not form solutions (e.g., alkali metals and metal powders.), and highly reactive reagents that require special handling to be used safely (such as organolithiums). The capabilities of the platform can be expanded by developing or purchasing special reactors, nitrogen-purged enclosures, and other engineering controls to safely handle these reagents. Despite 40% of proposed pathways being infeasible (Fig. 2C), the general nature of CASP implemented by ASKCOS means that there are usually proposed alternative pathways with accessible reactions, and only around 15% of candidates are removed from consideration.

The feasible candidate pathways are scored by their molecular value (the product of scaled prediction values and scaled ensemble variances) and relative platform feasibility (the product of inverse reagent cost, inverse pathway length, and compatibility of proposed reaction conditions with the well plate format) (supplementary materials, SM5). Only the highest scoring quartile of candidates are considered further (Fig. 2C). Any reagents required for the candidates that are not in the laboratory chemical inventory are rank ordered by the cumulative scores of the top 10 (exploration) or top one (exploitation) candidates that they are used to synthesize. The top-ranked reagent is added to the platform library and candidates that can be synthesized with the addition of the reagent are added to the selected products list. All remaining candidates are rescored and reagents reranked based on the updated library (Fig. 2D). The cycle of evaluation and selection is repeated until a predefined number of candidates are selected or the reagent budget is exhausted. Afterwards, the platform generates a document to prompt the operator to prepare stock solutions, specifying which vendors to purchase from and the minimum amount of material needed. The operator decides how to make stock solutions; solutions are prepared at high concentrations in solvents such as dimethylformamide, which would introduce 1 to 5% of stock solution solvent into the reaction, or at lower concentrations in volatile solvents such as chloroform, which would evaporate before the reaction begins. Completing this planning document serves as an optional managerial checkpoint for the operator to review the experiments to make sure that they will be safe.

Automation and experimental execution

Platform-selected reaction pathways are automatically translated (supplementary materials, SM6) into synthesis and characterization workflows to be executed in 96-well plates. Well plates offer ease of parallelization and sufficient material throughput (10 to 100 μmol scale) for multistep synthesis (*44*–*46*). The platform batches reactions into well plates on the basis of reaction temperature, reagent incompatibilities, and the order of reactions in multistep pathways. A finite sequence of temperatures that maximizes the number of selected pathways that can be completed is identified (Fig. 3A, plating), enabling multiple classes of reactions to be executed in the same well plate, and increasing throughput compared with the manual approach of grouping reactions by class alone. When this procedure leaves empty wells in a plate, the platform selects additional molecules that can be synthesized with the reagents in the platform library, increasing the use of the synthesis hardware and giving additional structures for property prediction model retraining with minimal additional experimental effort. Along with reaction execution tasks, high-level goal-oriented tasks to work up the reaction, analyze reaction outcomes, isolate target products, and characterize the isolated molecules are automatically generated, creating a series of platform jobs (Fig. 3A, organization). Four independent systems with different capabilities work simultaneously to accomplish these goal-oriented tasks while a master controller orchestrates tasks over a local network (Fig. 3A, experimental platform). Currently, the four systems are a liquid handler, a high-performance liquid chromatography (HPLC) with mass spectrometry instrument, a robotic arm, and a special processes unit that manages a storage carousel, a high-temperature reactor, a plate reader, and a photodegradation reactor.

Platform systems query two databases: a design database and a results database (supplementary materials, SM7). The design database tracks platform resources and is used by the platform systems to make real-time decisions on how to accomplish their assigned tasks. The results database manages experimental data and is used by the platform systems to record synthesis outcomes and molecular properties. The master controller schedules tasks to honor time constraints between tasks, adjusting to workflow changes made by the systems as needed (Fig. 3B). The occurrence of congestion on the platform necessitates additional rules for trafficking well plates between systems. Performance, a measure of platform efficiency (figs. S6 and S7; supplementary materials, SM7), is the percentage of well-based or plate-based operations, as appropriate, which did not generate an error requiring human intervention. For example, the HPLC analyzes the contents of every well, whereas the robotic arm moves an entire well plate at once, so their performances are evaluated per well and per plate, respectively. The performance of all systems exceeded 95% during the final 30 jobs for the exploration case study, which involved >1600 reactions (Fig. 3C) that were carried out across 910 hours of operations in a 5-month period. An analysis of the platform's performance is presented in the supplementary materials (SM7). It is important to note that although other high-throughput experimentation platforms can achieve higher throughputs (>1000 single-step reactions per day) for reaction condition screening, they do so for a narrow set of single-step reactions (e.g., C–C or C–N coupling) (*46*–*48*). The platform throughput is limited to ~200 reactions per day by HPLC analysis of reaction outcomes, but because of the wide scope of the workflows (prediction, execution, isolation, characterization, and model

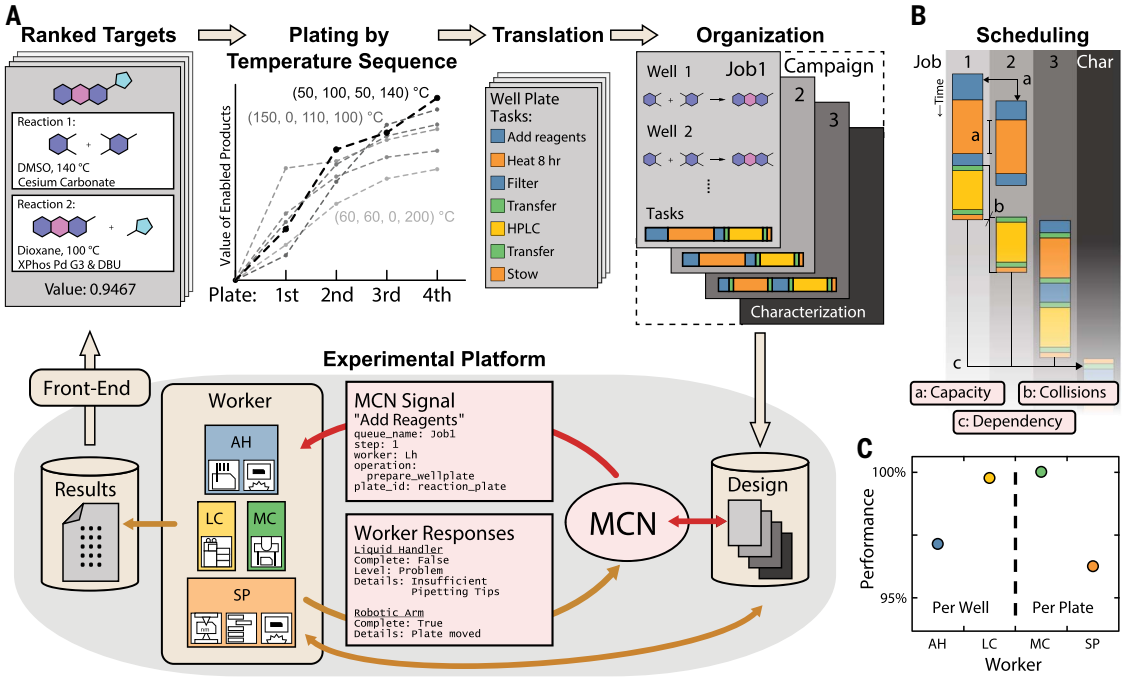

Fig. 3. Flow of information during experiment design, orchestration, execution, and data generation. (**A**) Platform-selected reactions from front-end predictions (Fig. 2) are batched into well plates, and the sequence of well plates with the highest value set of products is chosen (supplementary materials, SM5). Dashed lines are a guide to the eye to connect sequences of discrete temperatures. The well plate sequence is translated into a set of multistep goals and organized into lists of tasks for each well plate; the jobs are collated into a campaign and sent to the design database. The master control network (MCN) and databases mediate the flow of information from a campaign to the platform systems to the models for retraining. System legend: liquid handler and heater-shaker reactors (AH), blue; HPLC (LC), yellow; master controller and robotic arm (MC), green; plate reader, storage unit, and high-temperature and photodegradation reactors (SP), orange. (**B**) The initial scheduling of jobs in accordance with the scheduling algorithm: honoring (i) the capacity of a system to perform multiple tasks at once, (ii) the collision of resources between groups of tasks, and (iii) the dependencies between three synthesis jobs and a characterization job. (**C**) System performance (percent of steps not requiring human intervention) throughout the last 30 jobs of the exploration case study.

retraining), our realized throughput is lower and depends on the platform-selected chemistry. Other control architectures, such as those implemented in Chemputer (*49*, *50*) and ChemOS (*51*), were considered, but none supported parallel operation in well plates, work up and isolation, characterization, and the ability to modify workflows spontaneously. The described platform can perform multiple unrelated jobs in parallel and only requires human intervention for nonautomated error recovery and restocking (see "The role of the platform operator"; further detailed in supplementary materials, SM8).

To begin executing a job, the master controller checks that the first required system is available and that subsequent systems will have timely availability, ensuring that ongoing operations are not interrupted (Fig. 3B). Syntheses begin with reaction preparation in 96-well plates: The liquid handling robot finds the required reagents, dispenses them at appropriate volumes depending on stoichiometry and stock solution, and dispatches the reaction well plate to a reactor capable of the required reaction conditions [e.g., palladium-catalyzed reactions are sent to a nitrogen purged reactor; custom reactors are described in the supplementary materials (SM11)]. If the needed reagent is a product of a previous reaction, the volume dispensed is adjusted on the basis of the estimated reaction yield (supplementary materials, SM9). Reactions are run for 8 hours, which is excessive for faster reactions and inadequate for the most sluggish ones. Selecting an optimal duration for well plates containing many different reactions is not currently possible; quantitatively predicting kinetics for any proposed substrate, catalyst, and reagent combination is very challenging. How to predict more nuanced reaction conditions and durations for diverse reaction classes is an unsolved challenge that requires scalable predictions of chemical kinetics for complex molecules.

After executing reaction tasks, a series of automatically selected and executed work-up tasks process the crude products in preparation for ensuing reactions and HPLC analysis. Reactions with inorganic reagents such as carbonate or palladium complexes are extracted with chloroform and water in deep well plates, and all reactions are filtered through filter well plates. For intermediate products, a small sample (5 to 10%) of the filtered reaction is transferred to a new plate and diluted with dimethyl sulfoxide to dissolve the target products in a reverse-phase HPLC–compatible solvent. The reaction samples are transferred to the HPLC autosampler by the robotic arm and analyzed with a standardized water and acetonitrile gradient (supplementary materials, SM9). Reaction success was determined by identifying expected reaction product masses, and reaction yield was estimated from the HPLC chromatogram measured by the photodiode array detector. Operation and data export were automated through a vendor-supplied application-programming interface, and analysis occurred in real time (supplementary materials, SM9). For final products, the reaction outcome is analyzed in the same manner, but the majority of the filtered reaction is added to the HPLC analysis well plate. The retention time is used in a subsequent semipreparative HPLC run to isolate final products. The two-run method proved robust, but retention time prediction and real-time control of eluent composition could enable more efficient isolation without a prerequisite analytical run. Although not every product peak was baseline separated from by-products, our property assays capitalized on dye-molecule absorption of visible light, minimizing the influence of any ultraviolet-absorbing impurities on the property measurements. Although isolation of intermediate products is desirable, limitations of the current platform instruments make this impractical. Therefore, we used filtered intermediate reactions as feedstock for subsequent reactions, with around one-third of the multistep reaction pathways yielding the targeted final products. This success rate could be bolstered by preparative-scale HPLC purification but is not required to demonstrate autonomous molecular discovery. Given the limitations of small reaction scales and multistep reaction pathways, the operator must scale up reactions

and take NMR spectra off of the platform. Structural validation is a challenge for discovery-scale platforms but can be accomplished with NMR after interesting chemical spaces have been discovered.

For each property of interest, measurement and data processing protocols are defined beforehand (supplementary materials, SM9 and SM10) and are automatically applied to isolated products. Platform systems add measured data to the results database in real time for use when retraining the property prediction models. Absorption spectra are measured with a plate reader, partition coefficients are extracted from calibrated HPLC retention times, and photooxidative degradation rates are measured in a custom-built solar degradation device (supplementary materials, SM12). The device simulated sunlight at 10% solar intensity while periodically collecting absorption spectra in a plate reader; by quantifying the change in intensity of the pure sample spectrum deconvoluted from the measured spectrum, the rate of degradation could be extracted (supplementary materials, SM11). Additional properties can be measured with new hardware or workflows such as biological assays, and parallel implementation allows new hardware to work alongside existing hardware.

The role of the platform operator

Efforts toward realizing autonomous chemical discovery platforms have highlighted minimizing human intervention; however, human operators continue to have essential roles in the operation of these platforms. In this study, humans first need to set up platform goals and initialization operations (supplementary materials, SM8). During platform operation, operators oversee proposed experiments, help recover errors, and manage resources. One common source of platform errors requiring human intervention is hardware collision, which requires the operator to investigate the causes of the collision before reenabling the affected subsystems. These collisions arise from tight tolerances and robotic arm training drift that could be reduced by incorporating autocalibration equipment to preventively retrain positions. A particularly temperamental platform component is the HPLC, which requires an operator to bring it back online after errors such as clogged plumbing. Hardware or software solutions to improve robustness against common errors could be developed, such as analyzing which reactions lead to HPLC clogs and changing how those reactions are conducted. After set up, the platform proposes a series of experiments with operational plans. The operator may choose to review these proposed experiments to determine if they are safe to execute and whether they address the discovery goal well enough to invest platform time and resources; if not, the operator refines the goal or provides more tools to the platform. Afterwards, while the platform executes experiments, the operator is involved in platform resource management (keeping the platform stocked and purchasing and preparing stock material; supplementary materials, SM8). These managerial and custodial tasks are key factors that enable autonomous discovery and are often omitted when describing the operation of automated chemical platforms.

Despite progress, it is unlikely that human intervention will be completely removed from autonomous chemical discovery platforms in the near term and will continue to be a key point in ongoing conversations as autonomous platforms continue to advance. However, to assess autonomy in chemical discovery platforms (*52*, *53*), five items must ultimately be considered: (i) The scope and context of the discovery goal, (ii) the degree of choice afforded to the platform to accomplish the goal, (iii) the scale of real-time process-level feedback and adaptation, (iv) the manner in which experimental data informs future experiment design, and (v) the extent of platform automation. A detailed breakdown of these items is presented in the supplementary materials (SM8). As an illustrative comparison, specialized reaction optimization platforms are tasked to describe a reaction condition–yield landscape, but the scope of that discovery goal is narrow, and the experiment choices that can be made are highly constrained (adjustments to concentrations, temperatures, etc.) (*54*). These discovery tasks can be accomplished with fixed hardware configurations, minimal workflow flexibility, and can be guided by routine optimization algorithms. Although these platforms are self driving, their degree of autonomy is restricted to small, well-defined scopes and discovery goals. The platform we developed aims to explore general structure-property chemical spaces by leveraging the power of general machine learning predictive tools, only limited by safety considerations. As more chemistry is conducted by general-purpose autonomous discovery platforms, workflows and predictive models can be continually refined, further shifting the role of the operator toward supervision.

Exploration case study

Molecular exploration of chemical spaces beyond current datasets aims to identify productive spaces and determine whether molecules within those spaces have a set of desired properties. Property prediction models in these unexplored chemical spaces are uncertain because relevant training examples are not present to anchor predictions. To improve the property prediction models in these spaces, the platform first proposes a large number of candidates, then experimentally realizes several low-cost examples, and finally uses those examples to anchor future predictions. This approach allows the models to understand the chemical space with accessible chemistry and avoid investing excessive time and resources into synthetically complex, predicted high-performing molecules. With more accurate, anchored models, a further evaluation can narrow down the potential chemical space to a small number of hits for further exploration. This approach to molecular discovery is typical for identifying promising hit chemical spaces in hit-to-lead workflows.

To demonstrate molecular exploration, we prompted the platform to explore the properties of unexplored heterocyclic dye-like molecules. To find candidate scaffolds, we manually filtered ring structures with fewer than eight hits in the ZINC database (supplementary materials, SM1), as many molecular dye families are based around conserved, conjugated heterocyclic scaffolds (like xanthenes and coumarins). Cyclization reactions are critical to form heterocyclic structures but are challenging for retrosynthesis planners because multiple bonds form simultaneously (*55*). We manually inspected ASKCOS-recommended cyclization reactions for the ZINC hits to verify the ring-forming reaction templates and selected four heterocyclic structures to serve as exploration scaffolds (Fig. 4A). The graph-completion model automatically generated candidates by allowing any combination of C–H bonds on each scaffold to be functionalized (fig. S1). To explore the property space of these heterocyclic scaffolds, we prompted the platform to perform three rounds of molecular exploration. Beforehand, we provided a set of preferred-vendor chemical catalogs to the platform that, with the in-lab inventory, determined the domain of possible molecules. In each round, the platform considered property predictions, the practical constraints of reaction platform-feasibility, and reagent availability to select candidates to realize and characterize. Before starting subsequent rounds, the characterization data were used to update the property prediction models (discussion of the models follows in Fig. 5). The platform then used the retrained property models to drive a new iteration of the DMTA cycle.

Across the three rounds of exploration, the platform realized between 40 and 130 derivatives of each scaffold (Fig. 4A); the variation reflected differences in reaction fidelity. Recommended reaction pathways vary in length and retrosynthetic strategy, both between and within scaffolds. In some property space regions, the diversity and complexity required can be accessed by coupling commercial reagents together in single-step reactions. In other cases, starting materials with appropriate functional handles are available such that after forming the conserved heterocyclic scaffold, familiar reactions like palladium-catalyzed

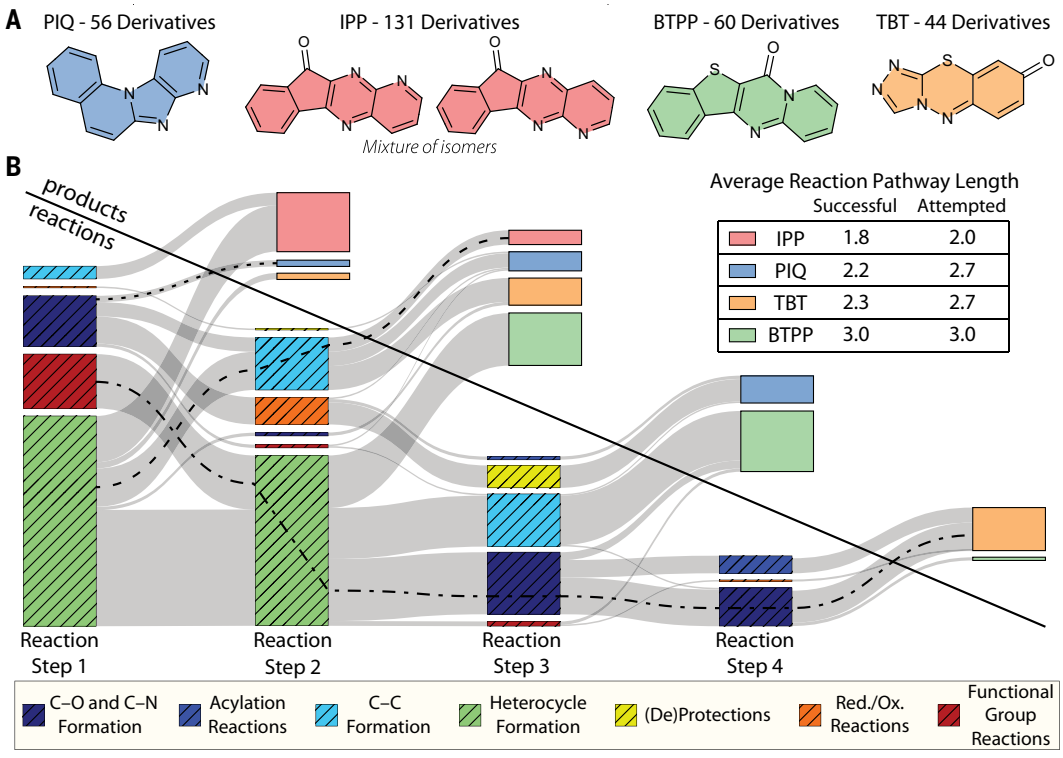

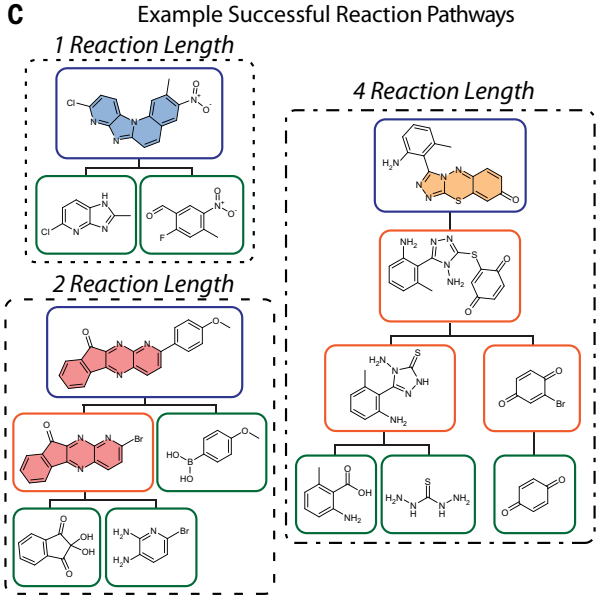

D Reaction Classes Selected

	IPP	PIQ	TBT	BTPP
C–O and C–N Formation	132/236	109/255	171/431	198/260
Acylation Reactions	0/12	10/39	16/46	5/13
C–C Formation	103/142	11/109	7/73	36/86
Heterocycle Formation	66/72	1/7	16/220	56/226
(De)Protections	2/8	0/1	6/6	---
Red./Ox. Reactions	4/8	4/46	---	---
Functional Group Reactions	47/141	11/73	20/234	23/86

Well Plate Numbers Used

Normal Well Plate	18	25	31	21
Filtration Plate	8	12	14	9
Deep Well Plate	17	14	18	6
Reactor Block Plate	4	6	4	5

Fig. 4. Chemistry predicted and attempted for the exploration case study. (**A**) Structures of the four scaffolds of interest explored by the platform: pyridoimidazoquinoline (PIQ), IPP, BTPP, and TBT. Shading color corresponds to the scaffold throughout the figure. (**B**) Diagram showing different products (solid bars, color coded by scaffold) synthesized by a variety of reaction types (hatched bars, color coded by reaction classification) and reaction pathway lengths. The sizes of the bars are proportional to the number of successful reactions and products. (**C**) Examples of successful reaction pathways for a derivative through a single-step pathway for the PIQ scaffold (dotted pathways), a two-step pathway for the IPP scaffold (dashed pathway), and a four-step pathway for the TBT scaffold (dash-dot pathway). An example of a successful three-step reaction pathway for the BTPP scaffold is shown in Fig. 2B. These example reaction pathways contain the cyclization strategy used to access each scaffold, as automatically planned by ASKCOS. Molecule box colors are the same as in Fig. 2. (**D**) The 37% overall reaction success rate broken down by class, scaffold, and number of attempts, and the number of well plates of different varieties needed to process those reactions.

cross couplings can be used to build the needed diversity and complexity. For more complex cases, reaction pathways begin by synthesizing reagents with appropriate functional handles before executing the critical cyclization reaction (Fig. 4B). When looking at the executed reaction pathways for each scaffold, the successful routes go through similar diversification strategies containing a key cyclization reaction (Fig. 4C). For each scaffold, a variety of reaction classes [based on the RXNO ontology (*56*)] were attempted to realize the automatically selected derivatives (Fig. 4D). The reaction success rate depends on the scaffold and reaction class. For example, a group of pathways that use a Friedel-Crafts acylation step were attempted for the indenopyridopyrazinone (IPP) derivatives (Fig. 4D), but the deactivated nature of the IPP scaffold prevented these reactions from succeeding. Such failure of chemistry did not halt the platform; rather, the reaction failure was recorded in the results database and dependent reaction pathways and characterizations were automatically disregarded in future operations. Varied reaction outcomes are often the result of insufficient specificity of reaction templates used in retrosynthesis planning or poor condition recommendations for uncommon reaction templates. Although outside of the scope of work presented, negative reaction outcomes could be used to improve retrosynthesis planning with each iteration. Similarly, successful cyclization reactions could be used to enhance model confidence when recommending those important reactions. Altogether, the platform selected 720 molecules to realize with an average pathway length of 2.6 reactions, requiring the platform to process 37 reaction

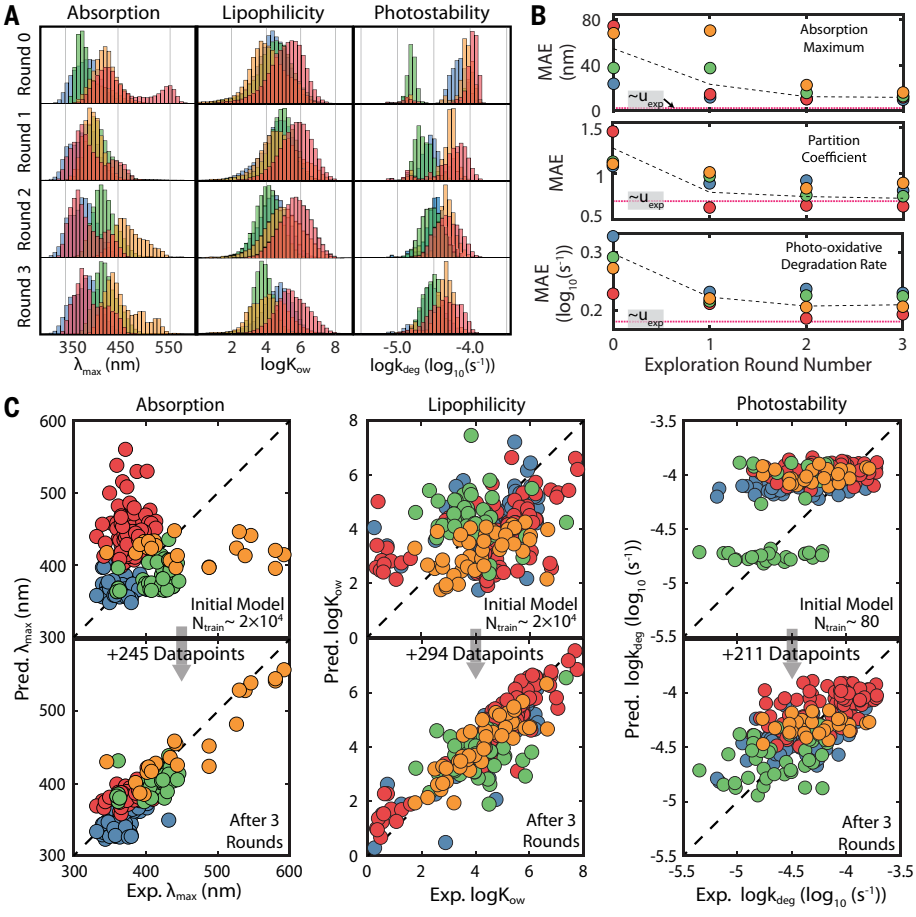

Fig. 5. Changes in property prediction models during iterative exploration. (**A**) Changes in the predicted property space with the general property model (Round 0) and following each round of exploration (Rounds 1 to 3). The shaded colors are based on scaffold coloring from Fig. 4 and apply to all subfigures. (**B**) Changes in the models' MAEs for each version of the λ_{max}, logK_{ow}, and logk_{deg} models evaluated by using cross-validation. Dashed black lines correspond to MAE values for all scaffolds combined. The experimental uncertainty (u_{exp}) is shown in each plot as a magenta dashed line. Exp., experimental; pred., predicted. (**C**) Comparison of predictions and experimental values for each of the property prediction models as initially trained and following three rounds of exploration. N_{train}, number of initial training molecules.

well plates and 181 additional well plates for workup and characterization (Fig. 4D), resulting in 294 previously unreported molecules being realized.

Property predictions for candidates made with initial property models (Fig. 5A, round 0) spanned a range of values and were relatively uncertain for the heterocyclic scaffolds of interest. These initial models were trained on datasets that were either extracted from literature or measured in house and contain no examples of the four scaffolds of interest. For exploration, the candidates that are most valuable are affordable, easy to synthesize, have properties that approach our target property space (redder absorbing, smaller partition coefficient, and photooxidatively stable), and have sizable prediction model ensemble variance (fig. S3 and supplementary materials, SM5). This approach favors diverse structures that move the derivatives' predicted properties toward the desired property space while providing information that will reduce the ensemble variance. As seen in Fig. 5, B and C, the absorption maximum, partition coefficient, and photooxidative degradation rates for the automatically realized and characterized molecules were substantially different from initial model predictions.

By iteratively and automatically realizing and measuring diverse derivatives, the platform learns about the structure-property space for the scaffolds of interest, improving the property prediction quality. Initial property prediction agreement with experimental values was subpar, with mean absolute errors (MAEs) of 52 nm for wavelength of maximum absorption, 1.3 for partition coefficient, and 0.30 $\log_{10}(s^{-1})$ for the rate of photooxidative degradation (Fig. 5B, round 0). The first round of exploration provided between 10 and 45 examples of each scaffold, depending on the complexity and success rate of the pathways for that scaffold. This handful of examples anchored the property models, shifting the predicted property space (Fig. 5A) and improving the models' MAEs (Fig. 5B), but the impact was not equal across properties or scaffolds. To investigate the impact of adding additional data, the platform performed two additional rounds of chemical exploration using the same candidate selection criteria but with updated property models and hence, candidate values, after each round. During three rounds of exploration—synthesizing 110, 110, and 90 molecules in the first, second, and third rounds, respectively—the property models improved for all scaffolds (Fig. 5, B and C), but the degree of improvement varied, and the impact of new data diminished for all property models with each round of exploration (Fig. 5B). For each property of interest, the number of experimental data points varied depending on the signal requirements for the assay. The partition coefficients were measured by using a calibrated retention time and were recorded for all identified products, resulting in 294 data points. Sufficient material had to be isolated to measure the absorption spectrum, and additional material was needed to measure the photooxidative degradation rate, resulting in 245 spectra and 211 first-order kinetic rate constants. Following the addition of the successful experimental data, the MAEs decreased to 11 nm, 0.7, and 0.21 $\log_{10}(s^{-1})$. For each of the scaffolds, the predicted property spaces (Fig. 5A) shifted toward ground-truth values as the property models learned about the structure-property spaces (Fig. 5, B and C), and for partition coefficients, the final MAE approached the limit imposed by experimental uncertainty.

Although the models' predictions improved for each scaffold, there was little change in predictive ability across general chemical spaces, demonstrating the local nature of these structure-property spaces. By verifying a handful of local experimental examples to anchor model predictions, candidate scaffolds that perform well can be more confidently considered for further examination. Initial property models both overpredicted [such as IPP absorption maxima or (triazolobenzothiadiazinone) TBT photooxidative degradation rate (Fig. 5)] and underpredicted [such as TBT or benzothienopyridopyrimidinone (BTPP) absorption maxima (Fig. 5)] the real performance of the candidate scaffolds depending on the local structure-property space. Despite a sizable number of datapoints from literature, the initial property models still did not extrapolate well to unexplored scaffolds. This exemplifies the challenge of relying only on generative and property-predicting models to guide molecular discovery, an ongoing challenge in untested chemical spaces.

Our platform overcomes this challenge by automatically designing and executing experiments with minimal human assistance, verifying interesting chemical spaces by first focusing on improving property-predicting models with relevant local examples before attempting complex and expensive molecular targets. For exploring these unknown chemical spaces, the ensemble variance appears to be a simple and effective metric to select regions about which the models are less confident for active learning campaigns. Looking more closely at each property, the absorption maximum and photooxidative stability predictions have larger ensemble variances than their corresponding experimental measurement variances, whereas the ensemble variances from the partition coefficient model prediction nearly match the experimental variances. As a result, as the accuracy of the partition coefficient model improves, its precision decreases (measured as ensemble variance), whereas for the other two models, accuracy and precision improve together. Although ensemble variance is a straightforward value to calculate and understand, as a new chemical space is explored, ensemble variance becomes a less efficient guide for properties with appreciable experimental error.

Exploitation case study

Property-predicting models can be exploited to realize potential top-performing molecules in chemical spaces containing preexisting data. Model exploitation naturally follows molecular exploration and is analogous to hit identification moving to lead optimization. Exploitation can be achieved on the same integrated platform as exploration by reweighting how candidates are valued. Predicted top performers are typically more synthetically complex and expensive, so rather than realizing several low-cost candidates, only a few confidently predicted top performers are selected.

To demonstrate model exploitation, we chose to optimize benzophenothiazinone (BPT) (Fig. 6A), a promising scaffold with sufficient cyclization yield and good model agreements in test experiments (fig. S15), a modest number of existing data points providing opportunity to discover new molecules, and structural similarities to other common dye families. We updated the property models with three examples of the scaffold to represent the promising hit and prompted the platform to discover lead molecules that simultaneously maximized absorption wavelengths, minimized partition coefficients, and minimized photodegradation rates (Fig. 6B). Although it is tempting to consider predicted property values alone when evaluating candidates (Fig. 6C), molecular generation is known to propose unusual structures (*39*) that may be outside the scope of property prediction models and have unrealistic predicted values. By considering model ensemble variance, synthetic accessibility score (*36*), and total reagent cost during candidate selection, the influence of out-of-scope structures can be minimized (Fig. 6C), thus valuing realistic candidates more highly and shifting values away from the optima idealistically defined by properties alone (Fig. 6B and fig. S4). The relative importance of these additional considerations can be weighted depending on acceptable tolerances to unusual chemical structures and prediction uncertainties in the candidate space.

The reaction pathways for the generated BPT derivatives all contain an established cyclization reaction involving the condensation of a halogenated naphthoquinone and a substituted 2-aminobenzenethiol (Fig. 6A). Several C–H sites on BPT were not accessible within a feasible number of reactions or from purchasable chemicals (Fig. 6A). From the generated derivatives, the platform automatically selected 14 of the highest-valued derivatives (Fig. 6B) to be realized, a selection of which are shown in Fig. 6C (remaining structures in SM13). Because of the air sensitivity of 2-aminobenzenethiol derivatives, the platform failed to realize some candidates that were attempted (fig. S13). For the nine candidates that were successfully realized and characterized, the predicted absorption maxima (MAE, 11 nm) and photooxidative degradation rate (0.4 log units) showed good agreement with experimental values, whereas the partition coefficient was consistently underpredicted by 2 log units. The performance of the BPT scaffold is appealing and could warrant continued investigation: It is structurally similar to phenoxazine dyes such as Nile blue, which was investigated for targeted delivery of photogenerated singlet oxygen (*57*) but is >10-fold more photooxidatively stable. Moreover, the molecules are fluorescent (fig. S9), suggesting the family might have additional photochemical activity to explore.

On inspection, the modest agreement of the partition coefficient values is not unexpected, as the derivatives that were selected by the platform all contain a primary aromatic amine. Although amine-containing derivatives can offer improved properties over amine-free derivatives, the prediction of their partition coefficients is challenging because their pK_a values (where K_a is the acid dissociation constant) can span a wide range, with charged species partitioning more into the aqueous phase. The partition coefficient model was not trained on enough aromatic amines to learn that the pK_a of 1-amino-BPT is too low for the derivatives to be ionized at the measured conditions. In practice, the partition coefficient of bioactive molecules is improved by introducing sulfonate groups that have sufficiently low pK_a values to be fully ionized in aqueous media. However, for our chemical space and properties of interest, amines strongly improve absorption maximum and photooxidative stability, whereas sulfonates only improve the partition coefficient. Because the importance of our properties of interest were equally weighted, the platform selected amine derivatives, improving two properties and modestly improving

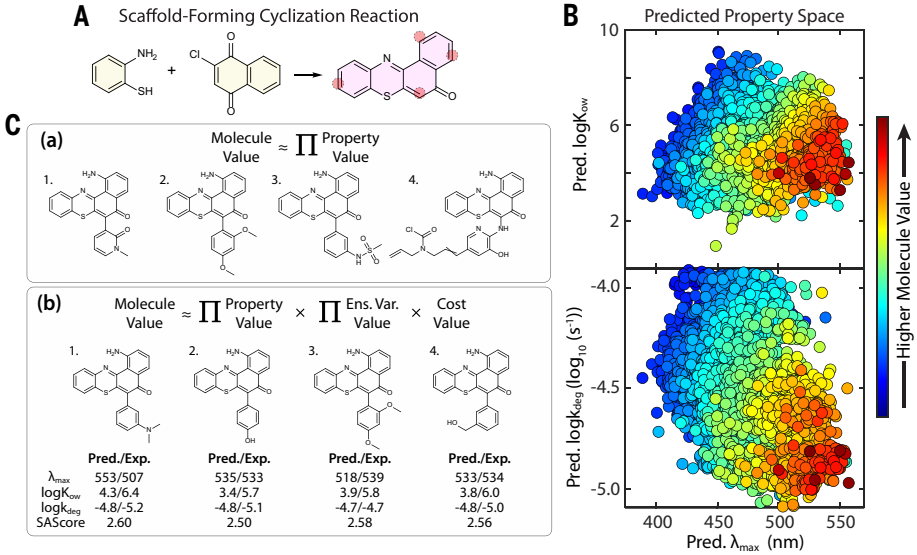

Fig. 6. Model exploitation case study. (**A**) Key cyclization reaction needed to access the ring-containing scaffold examined in the exploitation case study. Sites that were accessible with commercially available reagents in fewer than five reaction steps are highlighted in red. (**B**) Predicted property space of the generated candidates for logK_{ow} versus λ_{max} (top) and logk_{deg} versus λ_{max} (bottom). The color of each point reflects the candidate value in the exploitation workflow. (**C**) Two approaches to valuing candidates: (a) Idealistically considering only the predicted property values and (b) considering the predicted property value, ensemble variances (Ens. Var.), and cost. The top four most valuable molecules are shown for each valuation method.

the third. To maximize the improvement of the least improved property, a different selection function is needed, such as nondominated sorted or dynamic property weighting (*58*). Additionally, as the number of properties to consider grows, introducing property weightings will be advantageous to prioritize more critical properties, making new selection functions more desirable.

Conclusions

Discovery of molecules with targeted properties has historically been driven by manual experimentation, chemists' intuition, and an understanding of mechanisms and first principles. We have co-opted recently developed tools that assist chemists with the DMTA cycle to automatically explore chemical space and exploit known chemical structures. In the classic approach to the molecular discovery cycle, a hit molecule is altered to understand structure-function relationships; the platform we demonstrate does this without manual experimentation. The platform proposed, synthesized, and characterized 303 unreported dye-like molecules spread across four exploration scaffolds and one exploitation scaffold. The same integrated platform was able to both explore unknown structure-property spaces by searching for hit structures and exploit known structure-property spaces by optimizing lead structures. By the final rounds of operation, a typical job might encounter a single fault requiring operator intervention while preparing, executing, working up, and analyzing a well plate of up to 96 reactions (over the course of >1600 reactions). Although we present a general autonomous chemical discovery platform, there are areas in which autonomy can be further developed. There are cases in which human intervention can be further reduced by implementing existing, though often costly and less accessible equipment across the platform, such as commercial devices to dispense powders and prepare stock solutions. Additionally, the robust prediction of product distributions, by-products, and the corresponding solubilities in different environments would enable improved predictive purification and preemptive identification of potential experimental issues; however, these models do not exist. Reinforcement learning could also be used to develop a variety of workflows (*59*) that could help develop new operations or refine existing workflows, introducing a new dimension of platform adaptability for future versions of autonomous chemical discovery platforms.

Dye-like molecules represent a compelling property space and chemical space to explore and exploit; multistep syntheses applying a variety of chemical transformations are needed to access structures with a range of properties. The modular architecture of the integrated platform we demonstrated allows additional modules and workflows to be added as needed for different properties, such as biological activity, without impacting existing platform capabilities. Future iterations of the platform will benefit from improvements in predictive capabilities, particularly reaction fidelity, condition recommendation, and molecular generation, as well as analytical tools such as structural elucidation by means of HPLC or standalone detectors. The ongoing development of closed-loop integrated platforms is a promising path to continue accelerating molecular discovery.

Materials and methods

The following discussion summarizes the user workflow for an example scaffold (BTPP derivative from Fig. 2B). A more detailed description of autonomous candidate generation, candidate property evaluation and synthesis planning, model retraining, and all platform operations, including chemical handling, reaction preparation, execution, workup, and analysis, and product property analysis can be found in the provided supplementary materials.

Workflow initiation and platform operation (by a human operator)

The DMTA cycle must be instantiated by an operator who provides three configuration files to enable the workflow to run autonomously: (i) a set of Chemprop model parameters detailing each model's training, initial/literature data, and a specific goal for each property (maximize, minimize, or target a specific value), (ii) a scaffold from which to generate candidate molecules—in this work scaffolds were checked to ensure each had few literature precedents for discovery in unmapped chemical spaces—and (iii) a catalog of materials that can be handled by the automated synthesis machinery with associated costs and total budget. After starting the DMTA cycle, the operator must support the autonomous workflow by providing materials requested by the platform. Most requests entail providing chemicals not already in the platform library or not present in sufficient quantity; typically, such a request is fulfilled by refilling a solvent vessel or providing a stock solution in a septum-capped vial, either a 2-mL HPLC vial or 20-mL scintillation vial. Occasionally the platform may request restocking of consumable labware, such as well plates, lids, pipette tips, etc., but these are stored on-platform in sufficient quantity for multiple rounds of the DMTA cycle. When fulfilling requests, the operator enters identities and locations for labware and volumes and concentration for solutions into a platform-generated spreadsheet for easy updating of the platform library. Platform requests are made immediately before starting uninterruptible tasks, as scheduling and predicting material needs across multiple parallel and mutable jobs is impractical. Therefore, for the platform to run at capacity, an operator is required to monitor the system. On rare occasions, the operator may need to rectify an error such as a robotic collision; these events are almost always traced back to human error, such as placing a piece of labware in the wrong location but could be addressed with additional computer vision and advanced automated inventories, for example.

Chemprop model construction

Models for predicting molecule properties were all built using Chemprop, a software package available at https://github.com/chemprop/chemprop. For the larger dataset sizes of the absorption maximum and partition coefficient models, predictions were made using message-passing neural networks (MPNN) followed by conventional feed-forward networks. For small dataset sizes, random forest (RF) models have comparable or better performance than MPNNs. Therefore, the photooxidative degradation rate model was implemented with a RF within the Chemprop environment. Uncertainty was estimated with the variance of predictions from an ensemble of Chemprop models. Models were hyperparameter optimized before beginning the discovery campaign (training parameters can be found in table S2). Chemprop automatically implements the different model architectures, ensembling for uncertainty estimation, and hyperparameter optimization. To demonstrate the rate of discovery, either 10-fold or leave-one-out cross-validation was performed (depending on the number of new data points), although in operation, validation is not required as newly synthesized molecules will not be in the training data.

Candidate generation, reaction planning, and experiment selection

Methods for candidate generation, reaction planning, and experiment selection are covered in the main text (Front-end predictions) and supplementary materials (SM1 to SM6).

Reaction Execution and Workup

To achieve the desired reaction throughput, reactions were run in parallel in 96-well plates. All well plates were prepared with a Tecan Freedom Evo 200 liquid handler equipped with a liquid-handling (LiHa) arm, a multichannel arm (MCA), and a robotic manipulator (RoMa) arm that pipette individually addressed wells, pipette 96 wells in parallel, and move well plates, respectively. Additionally, workflows were developed for the RoMa to assemble and disassemble devices on the liquid handler bed, such as the Te-VacS microplate filtration system. Reaction groups taking place between 4° and 120°C were run on a

Inheho Teleshake or Thermoshake on the Tecan Evo bed. To accommodate the dilution and decrease in material with each step in a multistep synthesis, the platform multiplies the single step concentration (generally about 15 μmol) by the number of subsequent steps, so the first reaction in a three-step reaction would be prepared at 45 μmol, the second step at 30 μmol, and the final step at the desired 15 μmol. For air- and water-sensitive reaction groups, reactions were run on a dedicated Teleshake with a removable cover (by the RoMa) that has (replaceable) septa over each well and is constantly purged with nitrogen (supplementary materials, SM12), allowing pipetting into wells and heating to reaction temperatures with minimal exposure to air. For well plate compatibility, reactions taking place below 80°C were run in polypropylene well plates (1.8 mL working volume) while those above 80°C were run in Paradox aluminum well plates with glass inserts (0.8 mL working volume). A separate Precise Flex 400 collaborative robotic arm outside of the liquid handler was used to transfer well plates and resources between systems. Reactions beyond 120°C were run in a custom-made oven (supplementary materials, SM12) purged with nitrogen and sealed by means of an electric linear actuator uniformly pressing a fluorinated polymer film over an aluminum well plate with glass inserts (Para-dox Plate).

Crude reaction workup used the liquid handler to perform both extraction and filtration. For extraction, the target product is dissolved in chloroform and water is used to extract water-soluble impurities and salts. Use of chloroform ensures that the organic phase is on the bottom of the well and allows use of the MCA to extract all 96 wells at once without concern about the location of the boundary between the phases. Additionally, as chloroform is easily evaporated away with mild heating it is used to transfer material between wells, allowing the material to be redissolved in the predicted solvent. This is especially useful during filtration, which uses 96-well polypropylene filter well plates (0.45 μm) with the Te-VacS microplate filtration system to collect filtrate from each well. Filtration is required to prevent disruptions to HPLC operation. The reverse-phase HPLC system (water/acetonitrile gradient) cannot handle chloroform, so after filtration, an aliquot of the product is dissolved in dimethyl sulfoxide and the chloroform is evaporated.

HPLC was performed with a Shimadzu Nexera series system equipped with a photodiode array and mass spectrometer detectors and a well plate compatible autosampler. The mass spectrometer was used to identify target products, which were isolated as (nearly) pure material by collecting the product peak with a well plate compatible fraction collector. With a semipreparative HPLC column, enough material could be collected to assay the new molecules' properties of interest. As with the Tecan Evo, all operations of the Shimadzu Nexera were automated and coordinated by the master control network (supplementary materials, SM7).

Property Assays: Absorption maximum, partition coefficient, and photooxidative stability

Partition coefficients were determined with a calibrated HPLC retention time method (calibration and fitting data are presented in supplementary materials, SM10) based on an initial screen of 30 common molecules using the same gradient used for analytic screening. Absorption spectra were measured with a Tecan Spark plate reader. Sample well plates were loaded into and unloaded from the Spark by the RoMa. Spectral measurements were exported, and the raw and background-subtracted spectra were submitted to the experimental results database (control integration and data processing details can be found in supplementary materials, SM11). Photooxidative stability was measured with the Spark in conjunction with a custom-built reactor attached to the Spark on its second door. The reactor was purged with heated air (40°C) and utilized a forklift to hold the well plate under constant illumination, broad spectrum light from a xenon arc lamp (42 mW/m^2 average intensity). Periodically, the plate would be transferred back to the Spark for absorption spectra measurements. Using cumulative exposure time and estimated pristine compound spectrum tracking through spectral deconvolution (supplementary materials, SM11), a first-order degradation rate constant was determined for each sample.

Automated model retraining

Model retraining is automatically triggered after either a set period of time has elapsed or the platform completes a chemical discovery campaign. New data are appended to the initial training data and an ensemble of models is trained according to the configuration file, originally configured during the initial Chemprop model construction. Given the relatively small increase to the dataset from each round of discovery campaign, hyperparameters were not re-optimized when retraining the models, maintaining fast model retraining times. Additionally, high-performance computing resources through MIT SuperCloud for rapid model retraining and the updated models were returned to the prediction pipeline to start the next chemical discovery campaign.

REFERENCES AND NOTES

1. K. R. Campos *et al*., The importance of synthetic chemistry in the pharmaceutical industry. *Science* **363**, eaat0805 (2019). doi: 10.1126/science.aat0805
2. T. Dimitrov, C. Kreisbeck, J. S. Becker, A. Aspuru-Guzik, S. K. Saikin, Autonomous Molecular Design: Then and Now. *ACS Appl. Mater. Interfaces* **11**, 24825–24836 (2019). doi: 10.1021/acsami.9b01226; pmid: 30908004
3. M. Abolhasani, E. Kumacheva, The rise of self-driving labs in chemical and materials sciences. *Nat. Synth.* **2**, 483–492 (2023). doi: 10.1038/s44160-022-00231-0
4. E. Stach *et al*., Autonomous experimentation systems for materials development: A community perspective. *Matter* **4**, 2702–2726 (2021). doi: 10.1016/j.matt.2021.06.036
5. B. P. MacLeod, F. G. L. Parlane, A. K. Brown, J. E. Hein, C. P. Berlinguette, Flexible automation accelerates materials discovery. *Nat. Mater.* **21**, 722–726 (2022). doi: 10.1038/s41563-021-01156-3; pmid: 34907322
6. J. Peng *et al*., Human- and machine-centred designs of molecules and materials for sustainability and decarbonization. *Nat. Rev. Mater.* **7**, 991–1009 (2022). doi: 10.1038/s41578-022-00466-5
7. S. Langner *et al*., Beyond Ternary OPV: High-Throughput Experimentation and Self-Driving Laboratories Optimize Multicomponent Systems. *Adv. Mater.* **32**, e1907801 (2020). doi: 10.1002/adma.201907801; pmid: 32049386
8. E.-W. Lameijer, T. Bäck, J. N. Kok, A. P. Ijzerman, Evolutionary Algorithms in Drug Design. *Nat. Comput.* **4**, 177–243 (2005). doi: 10.1007/s11047-004-5237-8
9. Y. Kwon, S. Kang, Y.-S. Choi, I. Kim, Evolutionary design of molecules based on deep learning and a genetic algorithm. *Sci. Rep.* **11**, 17304 (2021). doi: 10.1038/s41598-021-96812-8; pmid: 34453086
10. M. Popova, O. Isayev, A. Tropsha, Deep reinforcement learning for de novo drug design. *Sci. Adv.* **4**, eaap7885 (2018). doi: 10.1126/sciadv.aap7885; pmid: 30050984
11. Z. Zhou, S. Kearnes, L. Li, R. N. Zare, P. Riley, Optimization of Molecules via Deep Reinforcement Learning. *Sci. Rep.* **9**, 10752 (2019). doi: 10.1038/s41598-019-47148-x; pmid: 31341196
12. S. K. Gottipati *et al*., Learning To Navigate The Synthetically Accessible Chemical Space Using Reinforcement Learning, *Proceedings of the 37th International Conference on Machine Learning*, July 13 to 18 2020, 3668–3679 (PMLR, vol. 119, 2020).
13. S. Kang, K. Cho, Conditional Molecular Design with Deep Generative Models. *J. Chem. Inf. Model.* **59**, 43–52 (2019). doi: 10.1021/acs.jcim.8b00263; pmid: 30016587
14. Chemprop: Molecular Property Prediction; https://github.com/chemprop/chemprop.
15. E. Heid *et al*., Chemprop: A Machine Learning Package for Chemical Property Prediction. ChemRxiv [Preprint] (2023); https://doi.org/10.26434/chemrxiv-2023-3zcfl-v2.
16. K. Yang *et al*., Analyzing Learned Molecular Representations for Property Prediction. *J. Chem. Inf. Model.* **59**, 3370–3388 (2019). doi: 10.1021/acs.jcim.9b00237; pmid: 31361484
17. ASKCOS; https://github.com/ASKCOS/.
18. C. W. Coley *et al*., A robotic platform for flow synthesis of organic compounds informed by AI planning. *Science* **365**, eaax1566 (2019). doi: 10.1126/science.aax1566; pmid: 31395756
19. T. Klucznik *et al*., Efficient Syntheses of Diverse, Medicinally Relevant Targets Planned by Computer and Executed in the Laboratory. *Chem* **4**, 522–532 (2018). doi: 10.1016/j.chempr.2018.02.002
20. P. Schwaller *et al*., Predicting retrosynthetic pathways using transformer-based models and a hyper-graph exploration strategy. *Chem. Sci.* **11**, 3316–3325 (2020). doi: 10.1039/C9SC05704H; pmid: 34122839
21. S. Genheden *et al*., AiZynthFinder: A fast, robust and flexible open-source software for retrosynthetic planning. *J. Cheminform.* **12**, 70 (2020). doi: 10.1186/s13321-020-00472-1; pmid: 33292482
22. J. Li *et al*., Synthesis of many different types of organic small molecules using one automated process. *Science* **347**, 1221–1226 (2015). doi: 10.1126/science.aaa5414; pmid: 25766227
23. S. H. M Mehr, D. Caramelli, L. Cronin, Digitizing chemical discovery with a Bayesian explorer for interpreting reactivity data. *Proc. Natl. Acad. Sci. U.S.A.* **120**, e2220045120 (2023). doi: 10.1073/pnas.2220045120; pmid: 37068251
24. A. C. Bédard *et al*., Reconfigurable system for automated optimization of diverse chemical reactions. *Science* **361**, 1220–1225 (2018). doi: 10.1126/science.aat0650; pmid: 30237351
25. A. M. K. Nambiar *et al*., Bayesian Optimization of Computer-Proposed Multistep Synthetic Routes on an Automated Robotic Flow Platform. *ACS Cent. Sci.* **8**, 825–836 (2022). doi: 10.1021/acscentsci.2c00207; pmid: 35756374
26. B. P. MacLeod *et al*., Self-driving laboratory for accelerated discovery of thin-film materials. *Sci. Adv.* **6**, eaaz8867 (2020). doi: 10.1126/sciadv.aaz8867; pmid: 32426501

27. T. Li *et al*., An automated platform for the enzyme-mediated assembly of complex oligosaccharides. *Nat. Chem.* **11**, 229–236 (2019). doi: 10.1038/s41557-019-0219-8; pmid: 30792508
28. P. C. Kotsias *et al*., Direct steering of de novo molecular generation with descriptor conditional recurrent neural networks. *Nat. Mach. Intell.* **2**, 254–265 (2020). doi: 10.1038/s42256-020-0174-5
29. B. Mikulak-Klucznik *et al*., Computational planning of the synthesis of complex natural products. *Nature* **588**, 83–88 (2020). doi: 10.1038/s41586-020-2855-y; pmid: 33049755
30. S. Steiner *et al*., Organic synthesis in a modular robotic system driven by a chemical programming language. *Science* **363**, eaav2211 (2019). doi: 10.1126/science.aav2211; pmid: 30498165
31. S. H. M. Mehr, M. Craven, A. I. Leonov, G. Keenan, L. Cronin, A universal system for digitization and automatic execution of the chemical synthesis literature. *Science* **370**, 101–108 (2020). doi: 10.1126/science.abc2986; pmid: 33004517
32. G. Pizzuto, J. De Berardinis, L. Longley, H. Fakhruldeen, A. I. Cooper, SOLIS: Autonomous Solubility Screening using Deep Neural Networks, *Proceedings of the International Joint Conference on Neural Networks*, 18 to 23 July 2022, (IEEE, 2022). doi: 10.1109/IJCNN55064.2022.9892533
33. B. Burger *et al*., A mobile robotic chemist. *Nature* **583**, 237–241 (2020). doi: 10.1038/s41586-020-2442-2; pmid: 32641813
34. W. Jin, R. Barzilay, T. Jaakkola, Hierarchical Generation of Molecular Graphs using Structural Motifs, *ICML'20: Proceedings of the 37th International Conference on Machine Learning*, July 2020, 4839–4848 (PMLR, 2020).
35. A. Gaulton *et al*., ChEMBL: A large-scale bioactivity database for drug discovery. *Nucleic Acids Res.* **40** (D1), D1100–D1107 (2012). doi: 10.1093/nar/gkr777; pmid: 21948594
36. P. Ertl, A. Schuffenhauer, Estimation of synthetic accessibility score of drug-like molecules based on molecular complexity and fragment contributions. *J. Cheminform.* **1**, 8 (2009). doi: 10.1186/1758-2946-1-8; pmid: 20298526
37. C. W. Coley, L. Rogers, W. H. Green, K. F. Jensen, SCScore: Synthetic Complexity Learned from a Reaction Corpus. *J. Chem. Inf. Model.* **58**, 252–261 (2018). doi: 10.1021/acs.jcim.7b00622; pmid: 29309147
38. A. Thakkar, V. Chadimová, E. J. Bjerrum, O. Engkvist, J.-L. Reymond, Retrosynthetic accessibility score (RAscore) - rapid machine learned synthesizability classification from AI driven retrosynthetic planning. *Chem. Sci.* **12**, 3339–3349 (2021). doi: 10.1039/D0SC05401A; pmid: 34164104
39. W. Gao, C. W. Coley, The Synthesizability of Molecules Proposed by Generative Models. *J. Chem. Inf. Model.* **60**, 5714–5723 (2020). doi: 10.1021/acs.jcim.0c00174; pmid: 32250616
40. H. Gao *et al*., Using Machine Learning To Predict Suitable Conditions for Organic Reactions. *ACS Cent. Sci.* **4**, 1465–1476 (2018). doi: 10.1021/acscentsci.8b00357; pmid: 30555898
41. G. Scalia, C. A. Grambow, B. Pernici, Y. P. Li, W. H. Green, Evaluating Scalable Uncertainty Estimation Methods for Deep Learning-Based Molecular Property Prediction. *J. Chem. Inf. Model.* **60**, 2697–2717 (2020). doi: 10.1021/acs.jcim.9b00975; pmid: 32243154
42. J. F. Joung, M. Han, M. Jeong, S. Park, Experimental database of optical properties of organic compounds. *Sci. Data* **7**, 295 (2020). doi: 10.1038/s41597-020-00634-8; pmid: 32901041
43. Y. Chung *et al*., Group Contribution and Machine Learning Approaches to Predict Abraham Solute Parameters, Solvation Free Energy, and Solvation Enthalpy. *J. Chem. Inf. Model.* **62**, 433–446 (2022). doi: 10.1021/acs.jcim.1c01103; pmid: 35044781
44. L. Gao *et al*., 'Chemistry at the speed of sound': Automated 1536-well nanoscale synthesis of 16 scaffolds in parallel. *Green Chem.* **25**, 1380–1394 (2023). doi: 10.1039/D2GC04312B; pmid: 36824604
45. A. Osipyan *et al*., Automated, Accelerated Nanoscale Synthesis of Iminopyrrolidines. *Angew. Chem. Int. Ed.* **59**, 12423–12427 (2020). doi: 10.1002/ange.202000887; pmid: 32048418
46. S. W. Krska, D. A. DiRocco, S. D. Dreher, M. Shevlin, The Evolution of Chemical High-Throughput Experimentation To Address Challenging Problems in Pharmaceutical Synthesis. *Acc. Chem. Res.* **50**, 2976–2985 (2017). doi: 10.1021/acs.accounts.7b00428; pmid: 29172435
47. A. C. Sun *et al*., A droplet microfluidic platform for high-throughput photochemical reaction discovery. *Nat. Commun.* **11**, 6202 (2020). doi: 10.1038/s41467-020-19926-z; pmid: 33273454
48. A. Bellomo *et al*., Rapid catalyst identification for the synthesis of the pyrimidinone core of HIV integrase inhibitors. *Angew. Chem. Int. Ed.* **51**, 6912–6915 (2012). doi: 10.1002/anie.201201720; pmid: 22689502
49. P. S. Gromski, J. M. Granda, L. Cronin, Universal Chemical Synthesis and Discovery with 'The Chemputer'. *Trends Chem.* **2**, 4–12 (2020). doi: 10.1016/j.trechm.2019.07.004
50. A. J. S. Hammer, A. I. Leonov, N. L. Bell, L. Cronin, Chemputation and the Standardization of Chemical Informatics. *JACS Au* **1**, 1572–1587 (2021). doi: 10.1021/jacsau.1c00303; pmid: 34723260
51. L. M. Roch *et al*., ChemOS: An orchestration software to democratize autonomous discovery. *PLOS ONE* **15**, e0229862 (2020). doi: 10.1371/journal.pone.0229862; pmid: 32298284
52. S. Lo *et al*., Review of Low-cost Self-driving Laboratories: The "Frugal Twin" Concept (2023; https://chemrxiv.org/engage/chemrxiv/article-details/64f94d43dd1a73847f598050).
53. R. B. Canty, B. A. Koscher, M. A. McDonald, K. F. Jensen, Integrating autonomy into automated research platforms. *Digit. Discov.* **2**, 1259–1268 (2023). doi: 10.1039/D3DD00135K
54. N. H. Angello *et al*., Closed-loop optimization of general reaction conditions for heteroaryl Suzuki-Miyaura coupling. *Science* **378**, 399–405 (2022). doi: 10.1126/science.adc8743
55. Y. Mo *et al*., Evaluating and clustering retrosynthesis pathways with learned strategy. *Chem. Sci.* **12**, 1469–1478 (2020). doi: 10.1039/D0SC05078D; pmid: 34163910
56. RXNO, reaction ontologies; https://github.com/rsc-ontologies/rxno.
57. M. Li *et al*., Near-Infrared Light-Initiated Molecular Superoxide Radical Generator: Rejuvenating Photodynamic Therapy against Hypoxic Tumors. *J. Am. Chem. Soc.* **140**, 14851–14859 (2018). doi: 10.1021/jacs.8b08658; pmid: 30362735
58. J. C. Fromer, C. W. Coley, Computer-aided multi-objective optimization in small molecule discovery. *Patterns (N. Y.)* **4**, 100678 (2023). doi: 10.1016/j.patter.2023.100678; pmid: 36873904
59. A. A. Volk *et al*., AlphaFlow: Autonomous discovery and optimization of multi-step chemistry using a self-driven fluidic lab guided by reinforcement learning. *Nat. Commun.* **14**, 1403 (2023). doi: 10.1038/s41467-023-37139-y; pmid: 36918561
60. B. A. Koscher, R. B. Canty, M. A. McDonald, K. F. Jensen, Autonomous, multi-property-driven molecular discovery: from predictions to measurements and back. Zenodo (2023), doi: 10.5281/zenodo.10037800
61. B. A. Koscher, R. B. Canty, M. A. McDonald, K. F. Jensen, Code for: Autonomous, multi-property-driven molecular discovery: from predictions to measurements and back. Zenodo (2023), doi: 10.5281/zenodo.10083815

ACKNOWLEDGMENTS

The authors thank the Shimadzu Innovation Center for their creation of the application programming interface which allowed programmatic control of the HPLC-MS and fraction collector. The authors thank the ASKCOS development team, particularly M. Liu, M. Murnin, M. Fortunato, and T. Struble for help with ASKCOS and the ASKCOS API. The authors acknowledge the MIT SuperCloud and Lincoln Laboratory Supercomputing Center for providing high-performance computing resources that have contributed to the research results reported within this report. The authors thank R. Alrufayi for help gathering the rules for implementation of reaction condition recommendations correction and P. Tumkur for developing Arduino code and the custom circuit board for the high-temperature thermal reactor. The authors thank A. Croke for help scaling up reaction workup. **Funding:** DARPA Accelerated Molecular Discovery (AMD) program under contract HR00111920025 and the MIT Consortium, Machine Learning for Pharmaceutical Discovery and Synthesis consortium (MLPDS). K.P.G. was supported by the National Science Foundation Graduate Research Fellowship Program under grant no. 1745302. **Author contributions:** Design, development, and supervised construction of the platform: B.A.K., R.B.C., M.A.M, and K.F.J.; Development, maintenance, and assembly of the robotic platform: B.J., T.H., and T.K.; Development and implementation of platform control and automation software: B.A.K., R.B.C., and M.A.M.; Design and development of property prediction models: K.P.G., C.J.M., H.W., F.H.V., and S.-C.L.; Development of automated property-prediction model retraining: K.P.G. and C.J.M.; Advisement on the development of property prediction models: R.G.-B. and W.H.G.; Design and development of graph-completion model: C.L.B. and W.J.; Advisement on the development of graph-completion model: T.S.J., R.B., and K.F.J.; Development of chemistry and assays and performance of experiments: B.A.K., R.B.C., and M.A.M.; Interpretation of results: all authors; Writing: B.A.K., R.B.C., and M.A.M.; Editing: all authors; Conceptualization, supervision of the project, and funding acquisition: T.S.J., R.B., R.G.-B., W.H.G., and K.F.J. **Competing interests:** The authors declare no competing interests. **Data and materials availability:** All data and code used in this study are freely available in the main text, supplementary materials, GitHub (https://github.com/RBCanty/MIT_AMD_Platform), and through Zenodo (*60, 61*), with the exception of the Shimadzu HPLC API, data from the CAS Content Collection, and Tecan Spark API, which are proprietary and unable to be publicly shared. For information on the Shimadzu API, contact the Shimadzu US Innovation Center (Columbia, MD; https://www.shimadzu.com/an/news-events/collabo/sicadl.html#lab01). For information on accessing the CAS Content Collection, contact the CAS Customer Center (https://www.cas.org/cas-data/cas-reactions). For information on the Tecan Spark API, contact your local Tecan Service Representative (https://www.tecan.com/contact-us). **License information**: Copyright © 2023 the authors, some rights reserved; exclusive licensee American Association for the Advancement of Science. No claim to original US government works. https://www.science.org/about/science-licenses-journal-article-reuse

SUPPLEMENTARY MATERIALS

science.org/doi/10.1126/science.adi1407
Materials and Methods
Supplementary Text
Figs. S1 to S17
Tables S1 to S5
References (*62*–*76*)

Submitted 5 April 2023; accepted 9 November 2023
10.1126/science.adi1407

Autonomous, multiproperty-driven molecular discovery: From predictions to measurements and back

Brent A. Koscher, Richard B. Canty, Matthew A. McDonald, Kevin P. Greenman, Charles J. McGill, Camille L. Bilodeau, Wengong Jin, Haoyang Wu, Florence H. Vermeire, Brooke Jin, Travis Hart, Timothy Kulesza, Shih-Cheng Li, Tommi S. Jaakkola, Regina Barzilay, Rafael Gómez-Bombarelli, William H. Green, and Klavs F. Jensen

Science **382** (6677), eadi1407. DOI: 10.1126/science.adi1407

Editor's summary

As chemists make increasing use of automated equipment and predictive synthesis algorithms, an autonomous research device is coming closer to realization. Koscher *et al*. developed a prototype platform for exploring the prospective dye-like properties of several polycyclic small-molecule classes. By combining machine learning–enabled planning and analysis with robotic reaction modules, the apparatus iteratively synthesizes variously substituted compounds to optimize their absorption properties, lipophilicity, and photo-oxidative stability. The authors elaborate on when and why human input still comes into play. —Jake S. Yeston